
This manuscript has been accepted for publication in the *Journal of Nuclear Materials*. Please note that, despite having undergone peer-review, the manuscript has yet to be formally published. Printed version may have slightly different content. The final version of this manuscript will be available via the ‘Peer-reviewed Publication DOI’ link. Please feel free to contact the corresponding author. Any feedback will be greatly appreciated.

1 **Effect of solution chemistry on the iodine release from iodoapatite in aqueous environments**

2 Zelong Zhang ^{†*}, Léa Gustin^{‡1}, Weiwei Xie[‡], Jie Lian[§], Kalliat T. Valsaraj^{||}, and Jianwei Wang^{†,⊥}

3 [†] Department of Geology and Geophysics, Louisiana State University, Baton Rouge, Louisiana
4 70803 United States

5 [‡] Department of Chemistry, Louisiana State University, Baton Rouge, Louisiana 70803 United
6 States

7 [§] Department of Mechanical, Aerospace, and Nuclear Engineering, Rensselaer Polytechnic
8 Institute, 110 Eighth Street, Troy, New York 12180, United States

9 ^{||} Cain Department of Chemical Engineering, Louisiana State University, Baton Rouge,
10 Louisiana 70803 United States

11 [⊥] Center for Computation and Technology, Louisiana State University, Baton Rouge, Louisiana
12 70803, United States

13 *Corresponding to zelongz@lsu.edu

14

¹ Current address: Department of Chemistry, University of Wisconsin-Madison, Madison, Wisconsin 53706, United States

15 **Abstract**

16 To ensure the safe disposal of nuclear waste, understanding the release process of radionuclides
17 retained in the nuclear waste forms is of vital importance. Iodoapatite $\text{Pb}_{9.85}(\text{VO}_4)_6\text{I}_{1.7}$, a potential
18 waste form for iodine-129, was selected as a model system for ceramic waste forms in this study
19 to understand the effect of aqueous species on iodine release. Semi-dynamic leaching tests were
20 conducted on bulk samples in cap-sealed Teflon vessels with 0.1 mol/L NaCl, Na_2CO_3 , Na_3PO_4 ,
21 and Na_2SO_4 solutions under 90 °C, fixed sample surface area to solution volume ratio of 5/m,
22 and periodic replacement of leaching solutions. The reacted solutions were then analyzed by
23 Inductively Coupled Plasma-Mass Spectrometry and Inductively Coupled Plasma-Optical
24 Emission Spectrometry; the leached surfaces were characterized by X-ray diffraction, scanning
25 electron microscopy, and infrared spectroscopy. The result shows that, compared to deionized
26 water, the ion-rich solutions enhanced the iodine release as a result of the increased ionic
27 strength, reduced activity coefficient of dissolved species, and increased solution pH. Surface
28 reactions can lead to the formations of secondary phases by ion-exchange and precipitation of
29 secondary phases. These findings suggest that an ion-rich environment in the geological
30 repository can be detrimental to the disposal safety of the apatite waste form.

31 **1 Introduction**

32 Nuclear power supplies low-carbon energy. The deployment of nuclear energy is motivated
33 by the pressing demand to mitigate climate change.¹ Sustainable development of the nuclear
34 energy requires concrete plans to safely dispose radionuclides waste generated by nuclear
35 fission.² Among those radionuclides, iodine-129 is particularly challenging to handle due to its
36 long half-life (15.7 million years), high yield (0.7% yield per fission of uranium-235),³ and weak
37 interactions with common materials in repository environments such as engineering barrier and
38 rock in geology formation.^{4,5} Iodide (I^-) is the most stable form of iodine in an environment with
39 pH and redox potential typically found in nature.⁶⁻⁸ Under highly oxidizing conditions, iodide
40 can be oxidized to iodine (I_2) and/or iodate (IO_3^-). All these iodine species are highly mobile in
41 nature given their high volatility and or high solubility.^{9,10} Iodine, as an essential element for
42 human health, can accumulate in human bodies.¹¹ For a healthy adult, 30% of the total iodine,
43 approximately 15-20 mg, is concentrated in the thyroid gland.¹² Chronical radiation from iodine-
44 129 beta decay can induce cancer to the thyroid follicular cells.¹¹ Therefore, the iodine-129 is a
45 primary contributor of the radiation dosage when analyzing the safety of disposal environments.⁴
46 The immobilization of iodine-129 is one of the critical research subjects for nuclear waste
47 management.^{4,13-18}

48 The most probable scenarios that compromise nuclear waste forms in a repository
49 environment are the contact with aqueous solutions.^{19,20} In a typical repository, nuclear waste
50 forms are packed into corrosion resistant metallic canisters underground.²¹ Canister corrosion
51 and degradation are anticipated to be the result of corrodents carried by groundwater.²² Through
52 infiltration and percolation of precipitation and groundwater aquifer, water can reach the
53 canisters and supply corrodents to react with the canister material. Upon the breaching of the

54 canister, the waste forms are exposed to an aqueous environment. Owing to the long half-life of
55 iodine-129, it is crucial to predict the long-term chemical durability of iodine waste forms. To
56 enable such prediction, it is necessary to obtain a fundamental understanding of corrosion
57 mechanisms of waste forms and how iodine in the host material is released in various solutions
58 that may occur under repository conditions.

59 Several waste form materials including glass, ceramics, glass-ceramics, cement, and
60 composite have been proposed to immobilize iodine.^{18,23} These waste forms immobilize iodine
61 via two major mechanisms: encapsulation and incorporation. To encapsulate iodine, the host
62 matrices need to contain iodine in a designated phase different from the host material. One
63 example is zeolite structure, in which iodine-bearing phases can be adsorbed on zeolite's
64 framework.^{17,24} Iodine can also be incorporated as a compositional element into the host matrix
65 structure through chemical bonding, such as iodoapatite $Pb_5(VO_4)_3I$ and sodalite
66 $Na_4(AlSiO_4)_3I$.^{13,25-27}

67 The difficulty to study the durability of different waste forms varies on a case-by-case basis.
68 It is particularly challenging to evaluate the encapsulation waste forms due to the complexity of
69 multi-phase and microstructures. On the other hand, characterizing the corrosion mechanism can
70 be relatively straightforward for single-phase crystal waste forms which have well-defined
71 crystal structures and simple microstructures. Based on the simplicity of its crystal structure and
72 microstructure, iodoapatite is chosen in this study as the model system of ceramic waste forms
73 that can incorporate radionuclides. In addition, apatite ceramics is a promising material due to its
74 thermal, mechanical, and chemical stability.^{13,25,28,29} These advantages are also demonstrated in
75 nature as apatite has been found as a retention matrix for actinides and fission products in natural
76 fission reactors at Franceville basin in Africa.^{22,30}

77 Several chemical durability tests have been performed on single-phase crystal waste forms.
78 Uno et al. in 2001 conducted soxhlet leach method on apatite $\text{Pb}_{10}(\text{VO}_4)_6\text{I}_2$.³¹ Soxhlet leach
79 method is designed to maximize the number of leachable constituents in leachant by allowing a
80 continuous contact between the waste and recycling leachant in a closed system.³² The iodine
81 release rate, $3.98 \times 10^{-5} \text{ g} \cdot \text{cm}^{-2} \cdot \text{d}^{-1}$, was reported.³¹ Guy et al. in 2002 studied apatite
82 $\text{Pb}_{10}(\text{VO}_4)_{4.8}(\text{PO}_4)_{1.2}\text{I}_2$ dissolution in aqueous solutions.³³ The resulting data shows that iodine
83 release was incongruent and exhibited dependency on temperature and pH. They also discovered
84 a secondary phase, lead vanado-phosphate, precipitated at the sample surface. Zhang et al. in
85 2007 performed static leaching test on $\text{Pb}_5(\text{VO}_4)_3\text{I}$ powder in a basic KOH/KHCO_3 buffer
86 solution.³⁴ Spectroscopic evidences show that OH^- and CO_3^{2-} can substitute I^- and VO_4^{3-} in
87 apatite. Maddrell et al. in 2014 conducted static leach tests on crushed powder iodide sodalite
88 $\text{Na}_4(\text{AlSiO}_4)_3\text{I}$ in KOH/KHCO_3 buffer solutions.²⁶ The result suggests a congruent dissolution.²⁶
89 Three leaching static experiments with durations of 3, 7, and 14 days exhibited a logarithmic
90 increase of iodine release. More recently, in 2017 Coulon et al. applied static leaching technique
91 to study the iodate-substituted hydroxyapatite in deionized water and groundwater.³⁵ They
92 reported that the iodine release is controlled by congruent dissolution under unsaturated
93 conditions and controlled by diffusion through ion exchange under saturated condition.
94 Interestingly, when groundwater was used as leachant, secondary phase hydroxyapatite
95 precipitated on the sample surface. Based on these studies, static leach test is a preferable method
96 to study the waste form durability due to the following reasons: 1) its simple procedure can
97 accommodate a wide range of test conditions; 2) the resultant data can be used to interpret the
98 release mechanism.³⁶ Static leaching method assumes that the solution feedback is negligible,
99 which is valid under conditions of sufficiently low surface to volume ratio.³⁶ However, the

100 solution feedback can gradually increase over time in a static leaching experiment. In cases
101 where the solution is oversaturated for phases of low solubility, secondary phases can precipitate
102 at the leached surface. Therefore, it can be problematic to use data from static leaching tests to
103 predict waste form behavior in a repository environment.³⁷ To address the issues of solution
104 feedback, a semi-dynamic leaching method was implemented by Zhang et al. in 2018 to quantify
105 the processes involved in the iodine release of an iodine-bearing apatite.²⁹ In their experiment,
106 deionized water solutions, as the leachant, were replaced periodically to minimize the solution
107 feedback. They demonstrated that iodine released from apatite is driven by short-term diffusion
108 and long-term matrix dissolution. This semi-dynamic approach was employed to produce
109 essential datasets to parameterize a mechanistic model suitable for predicting the kinetics of
110 iodine release under different conditions.³⁷

111 Since the aqueous systems in natural environment contain a variety of dissolved species, it is
112 necessary to understand how these aqueous species affect the iodine release from iodine waste
113 forms in an aqueous environment. For instance, the iodine release from apatite structured
114 materials can be enhanced by rapid substitution of halogen element³⁸⁻⁴¹ or inhibited by
115 precipitation of secondary phase.^{33,35,37} In this study, we conducted semi-dynamic leach tests on
116 single phase crystal ceramics of iodoapatite in 0.1 mol/L NaCl, Na₂CO₃, Na₃PO₄ and Na₂SO₄
117 solutions. The goal is to examine the impact of the solution chemistry on the kinetics of
118 iodoapatite dissolution. We hypothesized that dissolved aqueous species, via ion exchange and
119 precipitation, can substantially impact the dissolution kinetics; this effect should highly depend
120 on the chemistry of the aqueous species and the surface reactions of specific phases. The finding
121 of this study is expected to provide important insight into the long-term performance of iodine
122 waste forms and guidance to improve the disposal safety of nuclear waste.

123 **2 Experimental**

124 **2.1 Materials and methods**

125 The samples, obtained from previous studies,²⁵ were dense ceramic chips in
126 quadrilateral shape: 4.7 – 10.3 millimeter long by 1.1 – 1.8 millimeter thick with a
127 chemical composition of $\text{Pb}_{9.85}(\text{VO}_4)_6\text{I}_{1.7}$ according to the EDS and X-ray diffraction
128 refinement, as shown in Figures 1, 2 and 4. The iodoapatite samples were synthesized by
129 using high energy ball milling (HEBM) and spark plasma sintering (SPS) techniques.
130 Sample surfaces were polished by 4000-grit sandpaper on a mechanical polishing wheel
131 lubricated with ethanol. Details of the synthesis and characterization of these samples
132 were reported previously in separate publications.^{25,29,37}

133 The leaching method was adopted from ASTM C1308 standard test, as described in
134 the previous study^{29,37}. Four parallel experiments were conducted simultaneously for 14
135 days in four different leaching solutions: 0.1 mol/L NaCl, 0.1 mol/L Na_2CO_3 , 0.1 mol/L
136 Na_3PO_4 , and 0.1 mol/L Na_2SO_4 . Sample surface area (m^2) to solution volume (m^3) ratios
137 (S/V) of all four tests were fixed and maintained at 5/m. The leached solutions were
138 replaced every 24 hours. All reactor vessels were weighed before and after each interval
139 to monitor the solution losses which were within 0.5 % of the initial solution mass. In
140 addition, a control test was conducted in deionized water under identical conditions for 7
141 days using the same protocol. All samples after leaching experiments were collected,
142 rinsed by deionized water and ethanol, and air-dried.

143 **2.2 Characterization**

144 The elements of interest in the leachate solutions are I, Pb, and V. The leached
145 solutions, depending on the solution chemistry, were analyzed by Inductively Coupled
146 Plasma-Mass Spectrometry (ICP-MS, PerkinElmer Elan 9000) and/or Inductively-
147 Coupled Plasma-Optical Emission Spectrometry (ICP-OES, SPECTRO Ametek Spectro
148 ARCOS). Two standard solutions from Inorganic Ventures were used in the solution
149 analysis: 1) $1.001 \pm 0.007 \mu\text{g/ mL}$ iodide in H_2O solution and 2) $1.000 \pm 0.007 \mu\text{g/ mL}$
150 lead and $1.000 \pm 0.006 \mu\text{g/ mL}$ vanadium in 1% HNO_3 solution. Solution chemistry at
151 equilibrium state such as pH, ionic strength, speciation, and activity were calculated by
152 Visual MINTEQ package.

153 Samples were characterized by Scanning Electron Microscopy (SEM), Infrared
154 spectroscopy (IR), and X-ray diffraction spectroscopy (XRD). SEM images were taken by
155 a FEI Quanta SEM system with FEI Versa 3D DualBeam. Infrared spectroscopy was
156 performed on a Thermo Nicolet Continuum Infrared Microscope under Specular
157 Reflection mode and transmission mode with a fixed incident angle and an aperture area
158 of 10 by 10 μm covering 4000 to 650 cm^{-1} at a spectral resolution of 2 cm^{-1} . XRD data
159 were collected from PANalytical Empyrean X-Ray Diffractometer equipped with
160 monochromated $\text{Cu-K}\alpha$ radiation ($\lambda = 1.5406 \text{ \AA}$), operated at 45 kV, 40 mA, a step size of
161 0.026° , and a scanning range from 5 to 100° .

162 The crystal structures were refined by Le Bail algorithm using Jana2006 program.⁴²
163 All parameters were refined by the least-squares method. The pseudo-Voigt function was
164 used as the peak profile function. Structural parameters of $\text{Pb}_{9.85}(\text{VO}_4)_6\text{I}_{1.7}$ measured by
165 Audubert et al. were used as initial input (hexagonal, space group P63/m, $a = b = 10.422$
166 \AA , $c = 7.467 \text{ \AA}$, $\alpha = \beta = 90^\circ$; $\gamma = 120^\circ$).⁴³

167 **3 Results**

168 **3.1 Leached surface characterization by SEM/EDS**

169 In Figure 1 (a-c), no changes observable by naked eyes occurred on the surfaces of
170 samples leached by NaCl and NaSO₄ solutions for 14 days, whereas white layers were
171 gradually formed on the sample surfaces leached by Na₂CO₃ and Na₃PO₄ solutions within
172 the first week of the experiments. The SEM images in Figure 1 (d-i) show that the surface
173 alterations on samples leached by NaCl and Na₂SO₄ solutions were moderate, similar to
174 the water leached surface. However, samples leached by Na₂CO₃ and Na₃PO₄ solutions
175 demonstrated significant surface corrosion and possible formation of new phases. The
176 surface leached by Na₂CO₃ exhibited large grains, while congregated structures of similar
177 size appeared on the surface leached by Na₃PO₄.

178 According to EDS analysis, the surface chemical compositions in Figure 2 indicate
179 considerable changes between the leached samples and the pristine one. The key features
180 of EDS spectrum of pristine iodoapatite are: a carbon peak at 0.3 keV from background
181 (carbon tape), an oxygen peak at 0.5 keV, a broad Pb band from 2.34 to 2.45 keV
182 shouldered with two small Pb peaks at 1.8 and 2.6 keV, three iodine peaks at 3.9, 4.2, and
183 4.5 keV, and vanadium peaks at 4.9 and 5.4 keV. Overall, the iodine peaks at 3.94 keV
184 are nearly diminished in the EDS spectra of all four leached surfaces. The samples
185 leached by NaCl and Na₃PO₄ exhibited a substantial amount of chloride and phosphorus
186 signals at 2.62 and 2.01 keV, respectively. On the sample leached by NaCl, the Pb peak at
187 2.62 keV is comparable to the Pb peak at 1.8 keV, while the 2.62 keV peaks of the rest
188 samples are much weaker than their corresponding 1.8 keV peaks. Carbon signal at 0.27

189 keV from Na₂CO₃ leached sample cannot be properly quantified due to the background
190 interference from carbon tape and the graphite impurity introduced during sample
191 synthesis. Sulfur EDS peak at 2.31 keV overlaps with the broad central peak of Pb at 2.34
192 keV. Na₂SO₄ leached surface exhibited no sulfur peak near 2.3 keV given the
193 resemblance of the band shape between the sample leached by Na₂SO₄ and the rest. We
194 noticed variations of carbon and oxygen EDS signals among these samples which were
195 induced by the instrumentation settings such as sample orientation and beam parameters.
196 Therefore, carbon and oxygen were not considered in the EDS analysis.

197 **3.2 Leached surface characterization by IR analysis**

198 The IR spectroscopy results are listed in Figure 3. All these four samples yielded two
199 main peaks near 750 and 890 cm⁻¹, which are attributed to V-O bond.³⁴ Pristine
200 iodoapatite and samples leached by water, Na₂SO₄, and NaCl showed nearly identical
201 spectra. Surfaces leached by Na₂CO₃ and Na₃PO₄ exhibited position shifts of these two
202 V-O peaks to the region of 700 to 900 cm⁻¹ and multiple new bands. Sample leached by
203 Na₂CO₃ yielded sharp bands near 785, 890, 960, 1200, and 1450 cm⁻¹, in which the broad
204 band at 1450 cm⁻¹ is attributed to the stretching vibration of CO₃²⁻.^{44,45} The Na₃PO₄
205 leached surface generated IR peaks near 785, 870, 950, 1110, 1420, 1800, and 2200 cm⁻¹,
206 in which some can be assigned to the PO₄³⁻ (e.g. ν_1 – 950 cm⁻¹, ν_3 – 1100 cm⁻¹).⁴⁴
207 Interestingly, both CO₃²⁻ and PO₄³⁻ leached surfaces showed visible OH⁻ stretching
208 vibration near 3500 cm⁻¹,^{34,44} which also occurred on water leached surface under IR
209 transmission mode.²⁹

210 **3.3 Leached surface characterization by XRD**

211 The XRD data are shown in Figure 4. All these leached samples demonstrated
212 substantial differences compared to the pristine sample. Based on the XRD pattern, these
213 leached samples can be categorized into two groups: I) surfaces leached by NaCl and
214 Na₂SO₄ solutions, the pristine, and water leached sample; II) surfaces leached by Na₂CO₃
215 and Na₃PO₄ solutions, which were similar to the standard hydroxylvanadinite. The XRD
216 patterns of Group I are alike, which indicates no substantial structural changes compared
217 to the pristine. The XRD patterns of Group II display enhanced peak splitting between
218 25° and 28°. The original peak splitting of the pristine sample reflects the apatite structure
219 deformation which accommodates the relatively large iodide incorporated in the apatite
220 framework. The peak splitting of Na₂SO₄ leached surface is slightly enhanced, compared
221 to the pristine, but is weaker than the water leached sample. Interestingly, NaCl leached
222 surface yielded a diminished splitting at 26° and a new peak occurred at 29°, later
223 identified as $1\bar{3}1$ shown in Figure 5. The Full Width at Half Maximum (FWHM) of XRD
224 from NaCl leached surface was considerably broadened to ~0.4° compared to ~0.2° from
225 other samples, which may be attributed to the peak overlapping resulting from the
226 presence of a secondary phase. Both Na₂CO₃ and Na₃PO₄ leached samples exhibited
227 nearly identical XRD pattern, resembling the pattern of standard hydroxylvanadinite
228 Pb₁₀(VO₄)₆(OH)₂. The two highest bands on Pb₁₀(VO₄)₆OH₂ standard are 112 and $1\bar{3}1$
229 with an order of intensity $I_{112} < I_{1\bar{3}1}$. Same bands 112 and $1\bar{3}1$ also have the highest
230 intensity on Na₂CO₃ and Na₃PO₄ leached samples, however, the intensity of 112 is higher
231 than that of $1\bar{3}1$, $I_{112} > I_{1\bar{3}1}$.

232 The Le Bail method was applied to obtain structural information from the XRD data.
233 Table 1 compares the refined lattice parameters between sample surfaces of different

234 conditions and standards. No noticeable changes occurred in the crystal structures of
235 samples leached by deionized water and Na₂SO₄ when compared to that of pristine
236 sample (their length of *a*-, *b*-, and *c*-axes are approximately ~10.4, ~10.4, and ~7.5 Å,
237 respectively). On the other hand, a ~0.2 Å contraction along both the *a*- and *b*-axes were
238 observed for the samples leached by Na₂CO₃ and Na₃PO₄ solutions while the *c*-axis
239 remains the same and is consistent with other samples at ~7.45 Å. The observed and
240 calculated diffraction patterns, the residual and the indices of the main reflections of NaCl
241 leached sample are shown in Figure 5. We identified a secondary phase vanadinite
242 Pb₅(VO₄)₃Cl, indicating the substitution of iodine by chlorine during NaCl leaching.

243 **3.4 Solution composition analysis by ICP-MS and ICP-OES**

244 The results of the solution analysis on the leachates collected from the leach tests are
245 shown in Figure 6. The release rates of iodine, lead, and vanadium are depicted as green
246 circles, blue squares, and red triangles, respectively. In Figure 6(a), iodine release in NaCl
247 solution gradually increased over time, reaching a maximum rate near 0.8 mmol/m²/d at
248 day 11, and then slightly decreased near the end of the 14-day test. The Pb and V release
249 exhibited similar patterns with a relatively high initial rate around 0.075 mmol/m²/d, then
250 gradually decreased, and eventually approached a plateau near 0.05 mmol/m²/d. In Figure
251 6(b), the release patterns of iodine and vanadium in Na₂CO₃ are similar: release rates
252 rapidly reached maximum near day 2 and then gradually decreased over time approaching
253 a plateau. However, the long-term rate of Pb in Na₂CO₃ appears to be constant. In Figure
254 6(c), the iodine release in Na₂SO₄ exhibited a high initial rate approximately 0.32
255 mmol/m²/d and then its rate gradually decreased, eventually approaching a plateau around
256 0.15 mmol/m²/d. Despite no high initial release, the Pb and V release patterns follow the

257 trend of iodine release: gradually decreased over time and then rebounded near day 10.
258 The Figure 6(d) describes the element release of iodoapatite in Na_3PO_4 , which shows
259 constant rates of ~ 4.5 , ~ 3.5 , and ~ 13 $\text{mmol/m}^2/\text{d}$ for the release for iodine, Pb, and V,
260 respectively. Due to the instrumentation limitation and sample consumption, only four
261 leachates from the Na_3PO_4 experiment was analyzed for their Pb content.

262 Leaching rates of I, Pb, and V based on the solutions analysis are compared in Figures
263 7(a-c), respectively. In general, leaching tests conducted in the ionic solutions present
264 significantly higher element release rates than those of deionized water in the order of
265 $\text{Na}_3\text{PO}_4 > \text{Na}_2\text{CO}_3 > \text{Na}_2\text{SO}_4 >$ water, except in the NaCl solution. In Figure 7(a), iodine
266 release from Na_3PO_4 , Na_2CO_3 , and Na_2SO_4 solutions exhibited a long-term leach pattern
267 similar to that of water leaching: started with a high initial release, then gradually
268 decreased, and eventually stabilized and reached a plateau. The iodine release in NaCl
269 solution, however, presents a different pattern: iodine rate increased from the beginning
270 of leach test to day 11, when the rate reached maximum and then stabilized. The release
271 rates of Pb and V from NaCl test are relatively constant but not higher than those of water
272 leached as shown in Figures 7(b, c).

273 The molar ratios in leachate solutions are illustrated in Figures 7 (d, e). Except for the
274 anomalous NaCl data, the long-term I/V ratios in Figure 7(d) fluctuate around the ratio of
275 water-leached sample within the range of [0.34, 1.02], which are higher than the
276 stoichiometric value 0.28. In Figure 7(e), the long-term Pb/V ratios of NaCl and Na_2SO_4
277 tests are 1.36 and 1.65, approximate to the stoichiometric value 1.64, whereas the long-
278 term ratios from Na_2CO_3 and Na_3PO_4 tests are 0.95 and 0.27, significantly lower than
279 1.64.

280 3.5 Overview of leaching rates in solutions

281 The phases of interest in this study are the aqueous solutions and the solid surfaces.
282 The leachate solution chemistry in Figure 7 shows that iodine release from the sample
283 leached by the NaCl solution has a distinctive pattern. For the other leach tests, the long-
284 term iodine rates (plateau region in Figures 6-7) are at least one magnitude higher than
285 that from water leaching. And the order of iodine leach rate, based on solution analysis in
286 Figure 7 (a), is consistent with the orders of Pb and V rates in Figure 7 (b, c): $R_{\text{Pb/V/I}}(\text{Na}_3\text{PO}_4) > R_{\text{Pb/V/I}}(\text{Na}_2\text{CO}_3) > R_{\text{Pb/V/I}}(\text{Na}_2\text{SO}_4) > R_{\text{Pb/V/I}}(\text{deionized water})$. In the
287 following section, we will analyze the anomalous result of NaCl leach test and then
288 explain how element release behaviors differentiate due to the different solution
289 chemistry, such as pH and ionic species.
290

291 4 Discussion

292 4.1 Anomaly of the sample leached by NaCl solution

293 Iodoapatite sample leached by 0.1 mol/L NaCl solution exhibited unique surface
294 phase composition and iodine release pattern. The XRD data in Figures 4 and 5 show
295 leached surface has no apparent splitting in the region from 25° to 28° (2θ) and a new
296 peak ($\bar{1}\bar{3}1$), attributed by a vanadinite phase. This anomaly suggests a reduced structural
297 distortion, which can be contributed by substituting iodide with smaller chloride. The
298 refinement in Figure 5 confirmed new phase vanadinite was formed on the surface, which
299 resembles the XRD pattern of iodoapatite $\text{Pb}_{9.85}(\text{VO}_4)_6\text{I}_{1.7}$. The XRD data is consistent
300 with the EDS result and solution analysis. The Pb EDS band at 2.6 keV, in Fig 2, is
301 comparatively enhanced due to the overlap by chlorine signal at 2.6 keV. The release

302 rates of iodine from the NaCl test in Figure 6(a) suggest the new phase was growing until
303 the equilibrium state was reached. A similar iodine release pattern was observed in a pH 4
304 semi-dynamic leaching experiment, in which the rate anomaly was caused by the
305 formation of a secondary phase.³⁷ The molar ratios of Pb/V in Figure 7(e) approximate to
306 the stoichiometric value 1.6, indicating a congruent dissolution of Pb and V. The variation
307 of I/V molar ratios in Figure 7(d) is consistent with that of iodine rates in Figure 6(a).
308 Both the I/V ratios and iodine rates suggest an incongruent release for iodine, unlike the
309 congruent Pb and V. The SEM images in Figures 1(b, e) show that both surfaces leached
310 by NaCl and deionized water share similar morphology. The new phase vanadinite
311 $Pb_5(VO_4)Cl$, confirmed by the XRD refinement, suggests ion-exchange process between
312 iodide and chloride. This postulation is supported by the solution and surface analysis that
313 1) a significant amount of iodine was released into NaCl solution while the Pb and V rates
314 are comparable to the data of water leach test as shown in Figures 6-7; 2) the surface
315 alteration revealed by SEM in Figure 1 and the surface chemistry by EDS in Figure 2
316 resemble those of deionized water. Interestingly, the structural deformation of the original
317 iodine-bearing apatite $Pb_{9.85}(VO_4)_6I_{1.7}$ appeared to be restored in the chlorine-substituted
318 structure vanadinite $Pb_5(VO_4)_3Cl$. Given that the ionic radius of chloride (Cl^- , 1.68 ± 0.19
319 \AA) is considerably smaller than that of iodide (I^- , $2.11 \pm 0.19 \text{\AA}$),⁴⁶ exchanging the iodide
320 with smaller chloride seems to have repaired the structural deformation.

321 **4.2 Effect of pH on iodine release and secondary phase formation**

322 The solution pH has a strong effect on the iodine release of the iodoapatite. Parameters
323 of the solution chemistry calculated by VMINTEQ are listed in Table 2. According to our
324 previous studies, iodoapatite dissolution in deionized water can be represented by the

325 congruent release of Pb and V.²⁹ In Figure 7 (b, c), the Pb and V rates from different
326 solutions are generally constant, indicating a constant-dissolution controlled process. The
327 overall dissolution rates from low to high appears to be: R (*deionized water*) < R
328 (Na_2SO_4) < R (Na_2CO_3) < R (Na_3PO_4), which corresponds to the solution pH values ~6.1,
329 ~6.2, ~10.3, and ~10.9 under 90 °C as listed in Table 2. Therefore, increasing pH from
330 neutral to basic can increase the iodine release by enhancing the overall dissolution of the
331 iodoapatite, which is consistent with previous experimental results on synthetic
332 iodoapatite and natural apatites^{33,47}. However, due to the secondary phase formed in
333 Na_2CO_3 solutions, the dissolution process was being continuously hindered by the
334 accumulating precipitates. Interestingly, the trend of iodine released in Na_2CO_3 solution
335 of pH 10.3 resembles that of leaching iodoapatite under pH 4.³⁷ Despite the rate
336 difference, both surfaces leached by pH 4 and pH 10.3 formed secondary phases
337 (chervetite and hydroxylvanadinite, respectively). Our previous study showed that the
338 equivalent long-term rate of iodine release under pH 6 is 8.1 mmol/m²/d, over two
339 magnitudes higher than that of the deionized water 0.036 mmol/m²/d.³⁷ Nevertheless, the
340 release rates of iodine leached by the solutions of non-neutral pH are at least one
341 magnitude higher than that of the neutral pH solutions due to the enhanced dissolution
342 process.

343 Surface characterizations indicate the presence of new phases under the basic
344 conditions. The XRD analysis in Figure 4 and Table 1 shows the surfaces leached by the
345 Na_2CO_3 and Na_3PO_4 solutions were dominated by secondary phases resembling
346 hydroxylvanadinite $Pb_{10}(VO_4)_6(OH)_2$. The SEM in Figure 1 reveals different grain shapes
347 and sizes from the water leached, while the EDS in Figure 2 demonstrates that iodine was

348 depleted on the surface. The solution analysis also supports the formation of new phase
349 given the similar element release pattern to that of pH 4 and incongruent Pb/V ratios far
350 away from the stoichiometric value. As shown in Figure 7, the leaching rates of all
351 elements are at least one magnitude higher than the water leach rates of corresponding
352 elements. The results from this study and those from relevant literature suggest that the
353 solution pH exerts significant effects on the dissolution rate and the secondary phase
354 formation in aqueous environments such as chervetite and hydroxyvanadinite precipitated
355 under acidic and basic conditions, respectively.^{37,48,49}

356 **4.3 Effect of ionic species on the dissolution rate**

357 In this study, dissolved species affected the sample dissolution process by increasing
358 the ionic strength in solution, which consequently reduced the activity coefficient of
359 dissolved species. As a result, saturation state and solution feedback were reduced, which
360 in return increased the dissolution rate.⁴⁷ Although the 0.1 mol/L Na₂SO₄ and 0.1 mol/L
361 NaCl solutions have approximately the same solution pH as deionized water, the
362 dissolution rates in these ionic solutions are significantly higher than that of the deionized
363 water. As shown in Table 2, 0.1 mol/L Na₂SO₄ solution gives total ionic strength of 0.26
364 mol/L, 0.1 mol/L NaCl solution 0.098 mol/L, and deionized water 2.04×10^{-6} mol/L close
365 to zero. The vast difference in ionic strength leads to different degrees of saturation state.
366 The activity coefficient of the major ions Na⁺, Cl⁻, and SO₄²⁻ in these ionic solutions are
367 ranging from 0.25 to 0.76, considerably lower than the major ions H⁺ and OH⁻ with a
368 respective activity coefficient 1.00 in the deionized water. The dissolution rate in 0.1
369 mol/L Na₂SO₄ solution is higher than the rate in the 0.1 mol/L NaCl solution and
370 deionized water under the same pH and reaction mechanism, as shown in Figure 7.

371 Moreover, the average release rate of iodine in Na₃PO₄ (pH 10.9) is about one magnitude
372 higher than that of Na₂CO₃ (pH 10.3) despite their similar pHs. The difference in rates can be
373 inferred from the difference in ionic strength: 0.29 mol/L for 0.1 mol/L Na₃PO₄ and 0.25
374 mol/L for Na₂CO₃ solution.

375 In addition, no substantial structure change happened to the sample leached by 0.1
376 mol/L Na₂SO₄ solution. It is unlikely that anion SO₄²⁻ can be incorporated into apatite
377 structure as there is no evidence from surface characterization and solution analysis to
378 support that. No structural change was detected by the XRD characterization. The SEM
379 images and EDS analysis in Figures 1 and 2 show that the Na₂SO₄ and water leached
380 surfaces have a similar grain size, surface morphology, and chemical composition. The
381 element release rates and ratios in Figure 7 and 8 demonstrate a similar leach behavior
382 between samples leached by Na₂SO₄ and deionized water. The similarities in surface
383 alteration and leaching behavior between samples leached by Na₂SO₄ and water suggest
384 that the iodine release in Na₂SO₄ solution was controlled by short-term diffusion and
385 long-term dissolution and the release of Pb and V is controlled by congruent dissolution.
386 No precipitated was observed on Na₂SO₄ leached surface, which is also similar to the
387 surface leached by water.

388 In terms of the surface precipitation, the SEM images in Figures 1 (c, f) reflect intense
389 surface alterations in the solutions of Na₃PO₄ and Na₂CO₃. The leached surfaces yielded
390 XRD patterns similar to the standard hydroxyvanadinite Pb₅(VO₄)₃(OH). However,
391 significant contractions of *a*- and *b*-axes as shown in Table 2 indicate the size of VO₄ site
392 was reduced, which could be caused by a substitution of smaller groups.⁵⁰ The IR
393 spectroscopy of the sample leached by Na₃PO₄ confirms the existence of P-O bond and

394 OH⁻. Furthermore, the EDS detected phosphorus signal, which also supports that PO₄
395 group was in VO₄ site. The molar ratios of Pb/V in Figure 7 show a deficiency of Pb
396 relative to V in Na₃PO₄ leaching test. These evidences suggest the precipitates are a
397 product of hydroxyvanadinite with mixed site: Pb₁₀(VO₄)_n(PO₄)_{6-n}(OH)₂. The site mixing
398 is possible since Pb₁₀(VO₄)_x(PO₄)_{6-x}(OH)₂ can occur during wet chemistry reactions under
399 similar conditions.⁴⁸ Carbonate is known to be incorporated into apatite structure by
400 substitution.⁵⁰⁻⁵³ Given that phosphate (PO₄³⁻, ionic radius 2.30 ± 0.42 Å)⁴⁶ can replace
401 vanadate in iodoapatite,⁴⁸ it is reasonable to presume that carbonate of a smaller ionic
402 radius (CO₃²⁻, 1.89 ± 0.19 Å)⁴⁶ can substitute vanadate in a similar crystal structure.
403 Therefore, the secondary phase formed on in the Na₂CO₃ solution is Pb₁₀(VO₄)₆₋
404 _m(CO₃)_{1.5m}(OH)₂.

405 **4.4 Mechanism of iodoapatite dissolution and surface reactions in aqueous** 406 **environments**

407 Figure 8 generalizes the mechanism of iodoapatite dissolutions with multiple
408 processes contributing to the iodine release. Our previous study on iodine release in
409 deionized water suggests that the iodine release is driven by short-term diffusion and
410 long-term dissolution.²⁹ Diffusion and dissolution are affected by various factors of the
411 solution chemistry, such as solution ionic strength, pH, and secondary phase formation
412 resulted from a supersaturation of the solution with respect to low solubility species. In
413 neutral pH solutions, the iodine release is subjected to the substitution of iodine by
414 anionic species in solution such as OH⁻ and Cl⁻. When dealing with solutions of
415 comparable pH, a higher ionic strength, due to the ionic content, can enhance the
416 dissolution by changing saturation conditions. Solution pH other than near neutral can

417 increase the dissolution by exponentially accelerating the dissolution process. The
418 resulting rapid dissolution can often lead to the precipitation of secondary phases when
419 the solution approaches the supersaturation state of low solubility phases. Possible
420 secondary phases include chervetite $\text{Pb}_2\text{V}_2\text{O}_7$ under acidic condition³⁷ and
421 hydroxylvanadinite $\text{Pb}_5(\text{VO}_4)_3\text{OH}$ under basic condition.

422 **5 Conclusions**

423 The present study of the effect of solution compositions on iodoapatite dissolution
424 suggests that the higher ionic strength can enhance its dissolution by decreasing the
425 activity coefficient of reacting aqueous species, and thus can promote iodine release from
426 apatite. Non-neutral pH conditions clearly enhance the dissolution rate and can often lead
427 to precipitations of secondary phases, such as chervetite and hydroxylvanadinite. The
428 secondary phase precipitation at the surfaces hinders the dissolution rate because it
429 reduces the available reacting surface area. However, the overall iodine release rates in
430 both basic and acidic solutions are exponentially higher than those in the near-neutral pH
431 conditions, especially in deionized water. These impacts of solution chemistry on
432 dissolution add complexities to the current understanding of dissolution kinetics which is
433 based on leaching experiments conducted solely in deionized water. This study suggests
434 that, compared to fresh water with low ion concentrations, high concentrations of aqueous
435 species commonly found in underground brines can compromise the chemical durability
436 of apatite waste form in a geological repository. For this specific waste form, maintaining
437 neutral pH and low ion content in aqueous solutions are important to ensure the disposal
438 safety of radioactive iodine. Since iodine is one of the most challenging radionuclides to

439 immobilize, building a comprehensive theoretical framework of iodine immobilization
440 can significantly advance the research in nuclear waste disposal safety.

441 **Conflicts of interest**

442 There are no conflicts to declare.

443 **Acknowledgements**

444 This work was supported as part of the Center for Performance and Design of Nuclear
445 Waste Forms and Containers, an Energy Frontier Research Center funded by the U.S.
446 Department of Energy, Office of Science, Basic Energy Sciences (DE-SC0016584). The
447 sample surface characterizations were carried out at the Shared Instrumentation Facilities
448 (SIF) and Center for Advanced Microstructures and Devices (CAMD) of Louisiana State
449 University. We thank our XRD & Geochemistry Lab Researcher Wanda LeBlanc for
450 operating XRD experiments at SIF and facilitating our experiments in Geochemistry Lab.
451 We also thank Dr. Orhan Kizilkaya from CAMD for his assistance on infrared
452 spectroscopy.

453 **Date Availability**

454 Data will be made available on request

455 **References**

- 456 (1) Climate Change 2014: Mitigation of Climate Change: Working Group III Contribution to the Fifth
457 Assessment Report of the Intergovernmental Panel on Climate Change; Intergovernmental Panel
458 on Climate Change, Edenhofer, O., Eds.; Cambridge University Press: New York, NY, 2014.
- 459 (2) Alley, W. M.; Alley, R. The Growing Problem of Stranded Used Nuclear Fuel. *Environ. Sci. Technol.*
460 **2014**, 48 (4), 2091–2096. <https://doi.org/10.1021/es405114h>.
- 461 (3) Nichols, A. L.; Verpelli, M.; Aldama, D. L. Handbook of Nuclear Data for Safeguards; INDC(NDS)--
462 0502; International Atomic Energy Agency, 2007.
- 463 (4) Ojovan, M. I.; Lee, W. E. 10 - Long-Lived Waste Radionuclides. In *An Introduction to Nuclear
464 Waste Immobilisation (Second Edition)*; Ojovan, M. I., Lee, W. E., Eds.; Elsevier: Oxford, 2014; pp
465 107–115. <https://doi.org/10.1016/B978-0-08-099392-8.00010-3>.
- 466 (5) Aimoz, L.; Wieland, E.; Taviot-Guého, C.; Dähn, R.; Vespa, M.; Churakov, S. V. Structural Insight
467 into Iodide Uptake by AFm Phases. *Environ. Sci. Technol.* **2012**, 46 (7), 3874–3881.
468 <https://doi.org/10.1021/es204470e>.
- 469 (6) Um, W.; Serne, R. J.; Krupka, K. M. Linearity and Reversibility of Iodide Adsorption on Sediments
470 from Hanford, Washington under Water Saturated Conditions. *Water Res.* **2004**, 38 (8), 2009–
471 2016. <https://doi.org/10.1016/j.watres.2004.01.026>.
- 472 (7) Coughtrey, P. J.; Thorne, M. C. Radionuclide Distribution and Transport in Terrestrial and Aquatic
473 Ecosystems. A Critical Review of Data; 1983; Vol. 1.
- 474 (8) Whitehead, D. C. The Distribution and Transformations of Iodine in the Environment. *Environ. Int.*
475 **1984**, 10 (4), 321–339. [https://doi.org/10.1016/0160-4120\(84\)90139-9](https://doi.org/10.1016/0160-4120(84)90139-9).
- 476 (9) Schwehr, K. A.; Santschi, P. H.; Kaplan, D. I.; Yeager, C. M.; Brinkmeyer, R. Organo-Iodine
477 Formation in Soils and Aquifer Sediments at Ambient Concentrations. *Environ. Sci. Technol.* **2009**,
478 43 (19), 7258–7264. <https://doi.org/10.1021/es900795k>.
- 479 (10) Shimamoto, Y. S.; Takahashi, Y.; Terada, Y. Formation of Organic Iodine Supplied as Iodide in a
480 Soil–Water System in Chiba, Japan. *Environ. Sci. Technol.* **2011**, 45 (6), 2086–2092.
481 <https://doi.org/10.1021/es1032162>.
- 482 (11) Fuge, R.; Johnson, C. C. Iodine and Human Health, the Role of Environmental Geochemistry and
483 Diet, a Review. *Appl. Geochem.* **2015**, 63, 282–302.
484 <https://doi.org/10.1016/j.apgeochem.2015.09.013>.
- 485 (12) Patrick, L. Iodine: Deficiency and Therapeutic Considerations. *Altern. Med. Rev.* **2008**, 13 (2), 116–
486 127.
- 487 (13) Audubert, F.; Carpena, J.; Lacout, J. L.; Tetard, F. Elaboration of an Iodine-Bearing Apatite Iodine
488 Diffusion into a Pb₃(VO₄)₂ Matrix. *Solid State Ion.* **1997**, 95 (1), 113–119.
489 [https://doi.org/10.1016/S0167-2738\(96\)00570-X](https://doi.org/10.1016/S0167-2738(96)00570-X).
- 490 (14) Garino, T. J.; Nenoff, T. M.; Krumhansl, J. L.; Rademacher, D. X. Low-Temperature Sintering Bi–Si–
491 Zn-Oxide Glasses for Use in Either Glass Composite Materials or Core/Shell 129I Waste Forms. *J.
492 Am. Ceram. Soc.* **2011**, 94 (8), 2412–2419. <https://doi.org/10.1111/j.1551-2916.2011.04542.x>.
- 493 (15) Krumhansl, J. L.; Nenoff, T. M. Hydrotalcite-like Layered Bismuth–Iodine–Oxides as Waste Forms.
494 *Applied Geochemistry* **2011**, 26 (1), 57–64. <https://doi.org/10.1016/j.apgeochem.2010.11.003>.
- 495 (16) Sava, D. F.; Garino, T. J.; Nenoff, T. M. Iodine Confinement into Metal–Organic Frameworks
496 (MOFs): Low-Temperature Sintering Glasses To Form Novel Glass Composite Material (GCM)
497 Alternative Waste Forms. *Ind. Eng. Chem. Res.* **2012**, 51 (2), 614–620.
498 <https://doi.org/10.1021/ie200248g>.
- 499 (17) Sava, D. F.; Rodriguez, M. A.; Chapman, K. W.; Chupas, P. J.; Greathouse, J. A.; Crozier, P. S.;
500 Nenoff, T. M. Capture of Volatile Iodine, a Gaseous Fission Product, by Zeolitic Imidazolate

501 Framework-8. *J. Am. Chem. Soc.* **2011**, 133 (32), 12398–12401.
502 <https://doi.org/10.1021/ja204757x>.

503 (18) Riley, B. J.; Vienna, J. D.; Strachan, D. M.; McCloy, J. S.; Jerden, J. L. Materials and Processes for
504 the Effective Capture and Immobilization of Radioiodine: A Review. *J. Nucl. Mater.* **2016**, 470,
505 307–326. <https://doi.org/10.1016/j.jnucmat.2015.11.038>.

506 (19) Frankel, G. S.; Vienna, J. D.; Lian, J.; Scully, J. R.; Gin, S.; Ryan, J. V.; Wang, J.; Kim, S. H.; Windl, W.;
507 Du, J. A Comparative Review of the Aqueous Corrosion of Glasses, Crystalline Ceramics, and
508 Metals. *npj Materials Degradation* **2018**, 2 (1), 15. <https://doi.org/10.1038/s41529-018-0037-2>.

509 (20) Faucon, P.; Adenot, F.; Jacquinet, J. F.; Petit, J. C.; Cabrillac, R.; Jorda, M. Long-Term Behaviour of
510 Cement Pastes Used for Nuclear Waste Disposal: Review of Physico-Chemical Mechanisms of
511 Water Degradation. *Cem. Concr. Res.* **1998**, 28 (6), 847–857. [https://doi.org/10.1016/S0008-](https://doi.org/10.1016/S0008-8846(98)00053-2)
512 [8846\(98\)00053-2](https://doi.org/10.1016/S0008-8846(98)00053-2).

513 (21) Frankel, G. S.; Vienna, J.; Lian, J. WastePD, an Innovative Center on Materials Degradation. *npj*
514 *Mater. Degrad.* **2017**, 1 (1), 5. <https://doi.org/10.1038/s41529-017-0002-5>.

515 (22) Chapman, N. A.; McKinley, I. G.; Smellie, J. a. T. The Potential of Natural Analogues in Assessing
516 Systems for Deep Disposal of High-Level Radioactive Waste; EIR--545; Eidgenossisches Inst. fuer
517 Reaktorforschung: Sweden, 1984.

518 (23) Kato, H.; Kato, O.; Tanabe, H. Review of Immobilization Techniques of Radioactive Iodine for
519 Geological Disposal. **2002**. <https://doi.org/10.11484/JAERI-Conf-2002-004>.

520 (24) Chapman, K. W.; Chupas, P. J.; Nenoff, T. M. Radioactive Iodine Capture in Silver-Containing
521 Mordenites through Nanoscale Silver Iodide Formation. *J. Am. Chem. Soc.* **2010**, 132 (26), 8897–
522 8899. <https://doi.org/10.1021/ja103110y>.

523 (25) Yao, T.; Lu, F.; Sun, H.; Wang, J.; Ewing, R. C.; Lian, J. Bulk Iodoapatite Ceramic Densified by Spark
524 Plasma Sintering with Exceptional Thermal Stability. *J. Am. Ceram. Soc.* **2014**, 97 (8), 2409–2412.
525 <https://doi.org/10.1111/jace.13101>.

526 (26) Maddrell, E.; Gandy, A.; Stennett, M. The Durability of Iodide Sodalite. *Journal of Nuclear*
527 *Materials* **2014**, 449 (1), 168–172. <https://doi.org/10.1016/j.jnucmat.2014.03.016>.

528 (27) Chong, S.; Peterson, J. A.; Riley, B. J.; Tabada, D.; Wall, D.; Corkhill, C. L.; McCloy, J. S. Glass-
529 Bonded Iodosodalite Waste Form for Immobilization of ¹²⁹I. *J. Nucl. Mater.* **2018**, 504, 109–121.
530 <https://doi.org/10.1016/j.jnucmat.2018.03.033>.

531 (28) Le Gallet, S.; Campayo, L.; Courtois, E.; Hoffmann, S.; Grin, Yu.; Bernard, F.; Bart, F. Spark Plasma
532 Sintering of Iodine-Bearing Apatite. *J. Nucl. Mater.* **2010**, 400 (3), 251–256.
533 <https://doi.org/10.1016/j.jnucmat.2010.03.011>.

534 (29) Zhang, Z.; Heath, A.; T. Valsaraj, K.; L. Ebert, W.; Yao, T.; Lian, J.; Wang, J. Mechanism of Iodine
535 Release from Iodoapatite in Aqueous Solution. *RSC Adv.* **2018**, 8 (8), 3951–3957.
536 <https://doi.org/10.1039/C7RA11049A>.

537 (30) Gauthier-Lafaye, F. 2 Billion Year Old Natural Analogs for Nuclear Waste Disposal: The Natural
538 Nuclear Fission Reactors in Gabon (Africa). *C. R. Phys.* **2002**, 3 (7), 839–849.
539 [https://doi.org/10.1016/S1631-0705\(02\)01351-8](https://doi.org/10.1016/S1631-0705(02)01351-8).

540 (31) Uno, M.; Shinohara, M.; Kurosaki, K.; Yamanaka, S. Some Properties of a Lead Vanado-
541 Iodoapatite Pb₁₀(VO₄)₆I₂. *J. Nucl. Mater.* **2001**, 294 (1), 119–122.
542 [https://doi.org/10.1016/S0022-3115\(01\)00462-7](https://doi.org/10.1016/S0022-3115(01)00462-7).

543 (32) National Research Council. Scho; 2011. <https://doi.org/10.17226/13100>.

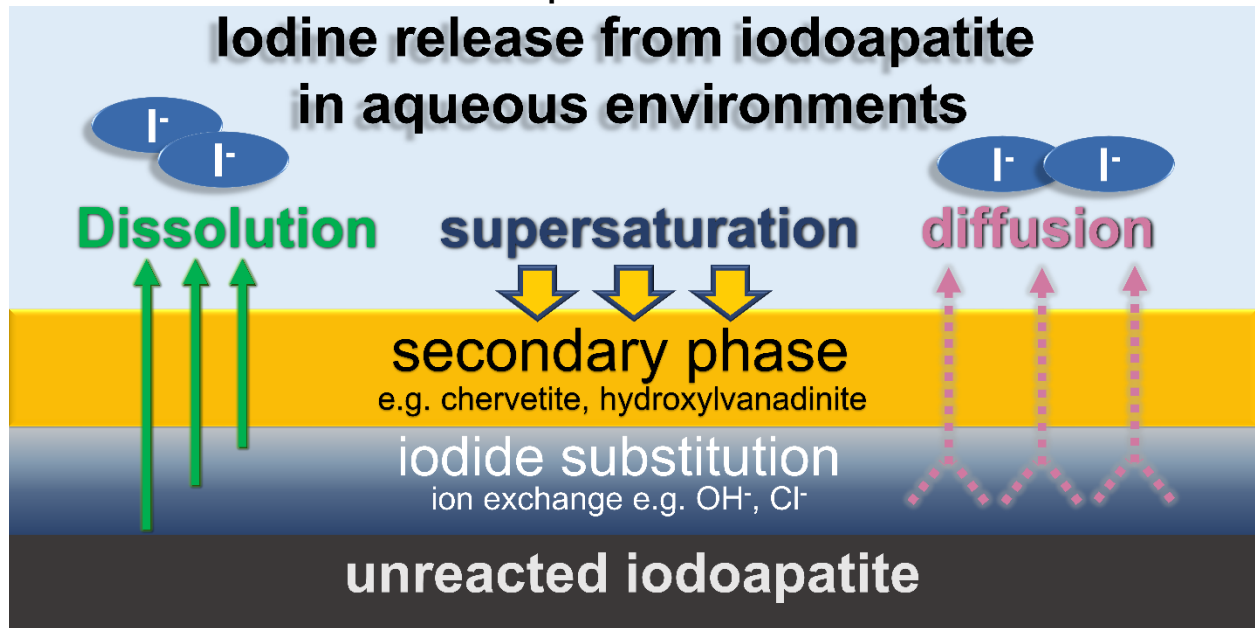
544 (33) Guy, C.; Audubert, F.; Lartigue, J.-E.; Latriille, C.; Advocat, T.; Fillet, C. New Conditionings for
545 Separated Long-Lived Radionuclides. *C. R. Phys.* **2002**, 3 (7), 827–837.
546 [https://doi.org/10.1016/S1631-0705\(02\)01377-4](https://doi.org/10.1016/S1631-0705(02)01377-4).

- 547 (34) Zhang, M.; Maddrell, E. R.; Abraitis, P. K.; Salje, E. K. H. Impact of Leach on Lead Vanado-
548 Iodoapatite [Pb₅(VO₄)₃I]: An Infrared and Raman Spectroscopic Study. *Mater. Sci. Eng. B* **2007**,
549 137 (1), 149–155. <https://doi.org/10.1016/j.mseb.2006.11.003>.
- 550 (35) Coulon, A.; Grandjean, A.; Laurencin, D.; Jollivet, P.; Rossignol, S.; Campayo, L. Durability Testing
551 of an Iodate-Substituted Hydroxyapatite Designed for the Conditioning of 129I. *J. Nucl. Mater.*
552 **2017**, 484, 324–331. <https://doi.org/10.1016/j.jnucmat.2016.10.047>.
- 553 (36) ASTM C1220-17, Standard Test Method for Static Leaching of Monolithic Waste Forms for
554 Disposal of Radioactive Waste; ASTM International: West Conshohocken, PA, 2017.
- 555 (37) Zhang, Z.; Ebert, W. L.; Yao, T.; Lian, J.; Valsaraj, K. T.; Wang, J. Chemical Durability and
556 Dissolution Kinetics of Iodoapatite in Aqueous Solutions. *ACS Earth Space Chem.*
557 <https://doi.org/10.1021/acsearthspacechem.8b00162>.
- 558 (38) Zhu, Y.; Zhang, X.; Chen, Y.; Xie, Q.; Lan, J.; Qian, M.; He, N. A Comparative Study on the
559 Dissolution and Solubility of Hydroxylapatite and Fluorapatite at 25°C and 45°C. *Chem. Geol.*
560 **2009**, 268 (1), 89–96. <https://doi.org/10.1016/j.chemgeo.2009.07.014>.
- 561 (39) Cazalbou, S.; Eichert, D.; Ranz, X.; Drouet, C.; Combes, C.; Harmand, M. F.; Rey, C. Ion Exchanges
562 in Apatites for Biomedical Application. *J. Mater. Sci. Mater. Med.* **2005**, 16 (5), 405–409.
563 <https://doi.org/10.1007/s10856-005-6979-2>.
- 564 (40) Brenan, J. Kinetics of Fluorine, Chlorine and Hydroxyl Exchange in Fluorapatite. *Chem. Geol.* **1993**,
565 110 (1), 195–210. [https://doi.org/10.1016/0009-2541\(93\)90254-G](https://doi.org/10.1016/0009-2541(93)90254-G).
- 566 (41) Dorozhkin, S. V. A Review on the Dissolution Models of Calcium Apatites. *Prog. Cryst. Growth*
567 *Charact.* **2002**, 44 (1), 45–61. [https://doi.org/10.1016/S0960-8974\(02\)00004-9](https://doi.org/10.1016/S0960-8974(02)00004-9).
- 568 (42) Petříček, V.; Dušek, M.; Palatinus, L. Crystallographic Computing System JANA2006: General
569 Features. *Z. Kristallogr. Cryst. Mater.* **2014**, 229 (5), 345–352. <https://doi.org/10.1515/zkri-2014-1737>.
- 571 (43) Audubert, F.; Savariault, J.-M.; Lacout, J.-L. Pentalead Tris(Vanadate) Iodide, a Defect Vanadinite-
572 Type Compound. *Acta Crystallogr. C* **1999**, 55 (3), 271–273.
573 <https://doi.org/10.1107/S0108270198005034>.
- 574 (44) Ślósarczyk, A.; Paszkiewicz, Z.; Paluszkiwicz, C. FTIR and XRD Evaluation of Carbonated
575 Hydroxyapatite Powders Synthesized by Wet Methods. *J. Mol. Struct.* **2005**, 744–747, 657–661.
576 <https://doi.org/10.1016/j.molstruc.2004.11.078>.
- 577 (45) Merry, J. C.; Gibson, I. R.; Best, S. M.; Bonfield, W. Synthesis and Characterization of Carbonate
578 Hydroxyapatite. *J. Mater. Sci. Mater. Med.* **1998**, 9 (12), 779–783.
579 <https://doi.org/10.1023/A:1008975507498>.
- 580 (46) Roobottom, H. K.; Jenkins, H. D. B.; Passmore, J.; Glasser, L. Thermochemical Radii of Complex
581 Ions. *J. Chem. Educ.* **1999**, 76 (11), 1570. <https://doi.org/10.1021/ed076p1570>.
- 582 (47) Guidry, M. W.; Mackenzie, F. T. Experimental Study of Igneous and Sedimentary Apatite
583 Dissolution: Control of PH, Distance from Equilibrium, and Temperature on Dissolution Rates.
584 *Geochim. Cosmochim. Acta* **2003**, 67 (16), 2949–2963. [https://doi.org/10.1016/S0016-7037\(03\)00265-5](https://doi.org/10.1016/S0016-7037(03)00265-5).
- 586 (48) Cao, C.; Chong, S.; Thirion, L.; C. Mauro, J.; S. McCloy, J.; Goel, A. Wet Chemical Synthesis of
587 Apatite-Based Waste Forms – A Novel Room Temperature Method for the Immobilization of
588 Radioactive Iodine. *J. Mater. Chem. C* **2017**, 5 (27), 14331–14342.
589 <https://doi.org/10.1039/C7TA00230K>.
- 590 (49) Campayo, L.; Audubert, F.; Lartigue, J.-E.; Courtois-Manara, E.; Gallet, S. L.; Bernard, F.; Lemesle,
591 T.; Mear, F. O.; Montagne, L.; Coulon, A.; et al. French Studies on the Development of Potential
592 Conditioning Matrices for Iodine 129. *Mater. Res. Soc. Symp. Proc.* **2015**, 1744, 15–20.
593 <https://doi.org/10.1557/opl.2015.309>.

- 594 (50) Zapanta-Legeros, R. Effect of Carbonate on the Lattice Parameters of Apatite. *Nature* **1965**, 206
595 (4982), 403. <https://doi.org/10.1038/206403a0>.
- 596 (51) White, T. J.; Dong, Z. L. Structural Derivation and Crystal Chemistry of Apatites. *Acta Cryst. B*
597 **2003**, 59 (1), 1–16. <https://doi.org/10.1107/S0108768102019894>.
- 598 (52) Fleet, M. E.; Liu, X. Coupled Substitution of Type A and B Carbonate in Sodium-Bearing Apatite.
599 *Biomaterials* **2007**, 28 (6), 916–926. <https://doi.org/10.1016/j.biomaterials.2006.11.003>.
- 600 (53) Landi, E.; Tampieri, A.; Celotti, G.; Vichi, L.; Sandri, M. Influence of Synthesis and Sintering
601 Parameters on the Characteristics of Carbonate Apatite. *Biomaterials* **2004**, 25 (10), 1763–1770.
602 <https://doi.org/10.1016/j.biomaterials.2003.08.026>.
603

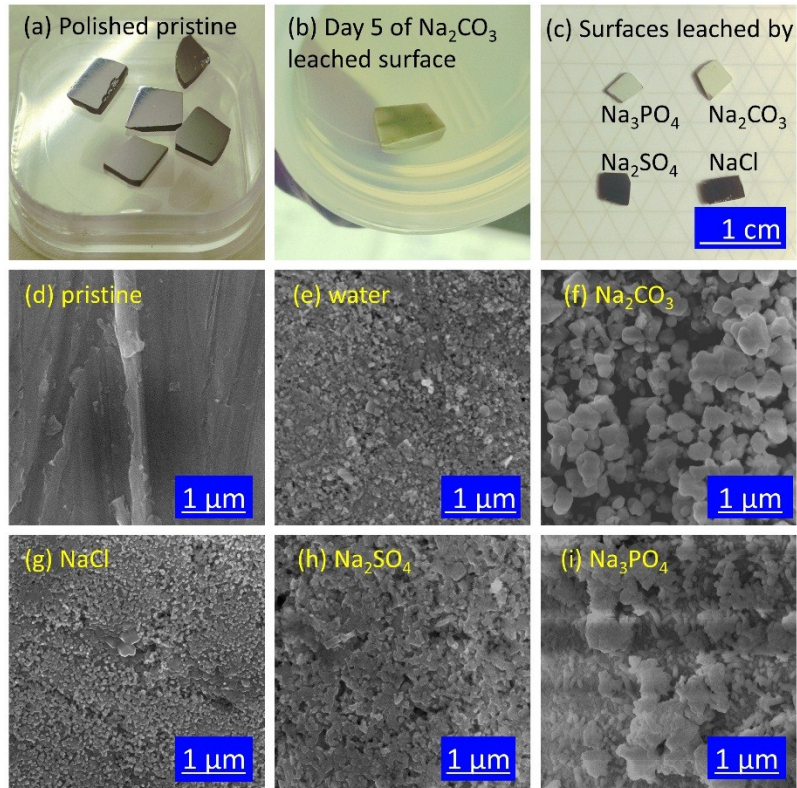
604

Graphical abstract



605

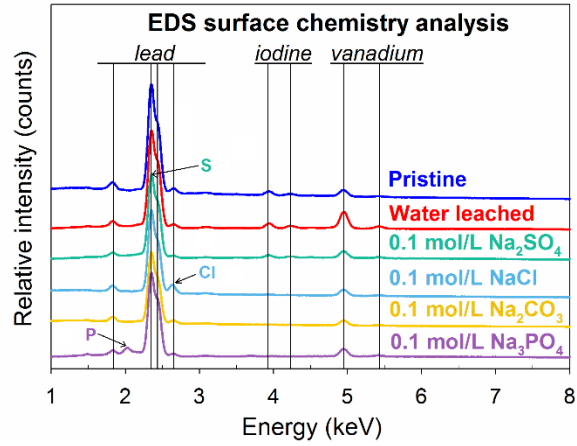
606



607

608 Figure 1.(a) Polished pristine iodoapatite samples before test, (b) iodoapatite leached
 609 surface during the 5th replacement of Na₂CO₃ solution, (c) surface leached by at the end
 610 of 14-day leaching tests, SEM images of (a) a polished pristine iodoapatite and the
 611 samples leached by (b) deionized water, (c) 0.1 mol/L Na₂CO₃, (d) 0.1 mol/L NaCl, (e)
 612 0.1 mol/L Na₂SO₄, and (f) 0.1 mol/L Na₃PO₄.

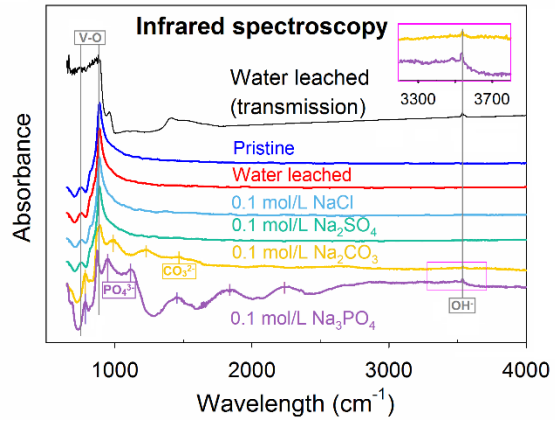
613



614

615 Figure 2. EDS spectra of a pristine iodoapatite and the samples leached by deionized
 616 water, 0.1 mol/L NaCl, 0.1 mol/L Na₂CO₃, 0.1 mol/L Na₃PO₄, and 0.1 mol/L Na₂SO₄
 617 solutions.

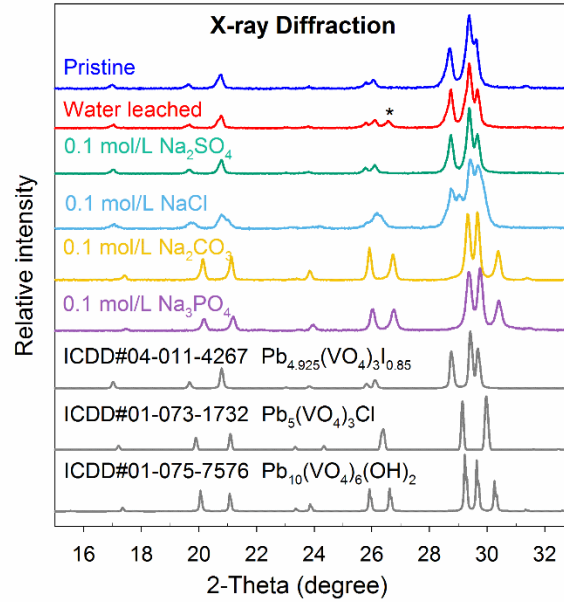
618



619

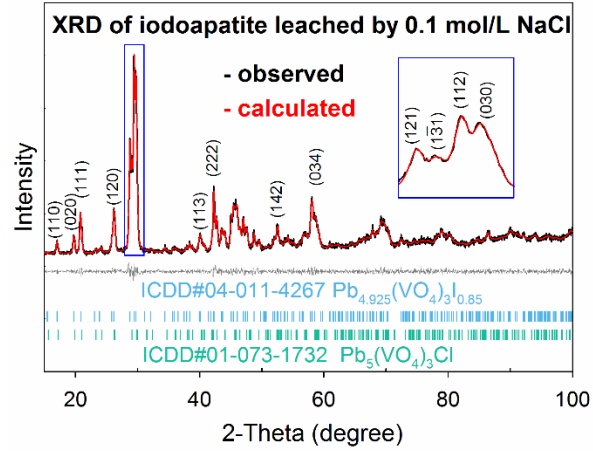
620 Figure 3. Infrared spectroscopy of pristine iodoapatite and leached samples by
 621 deionized water, NaCl, Na₂SO₄, Na₂CO₃, and Na₃PO₄ solutions.

622



623

624 Figure 4. XRD patterns of a pristine iodoapatite and the samples leached by deionized
 625 water, 0.1 mol/L Na₂SO₄, 0.1 mol/L NaCl, 0.1 mol/L Na₂CO₃, and 0.1 mol/L Na₃PO₄. In
 626 addition, standard XRD spectra of iodoapatite, vanadinite, and hydroxylvanadinite are
 627 listed for comparison. * denotes the graphite impurity introduced during sample
 628 synthesis.²⁵

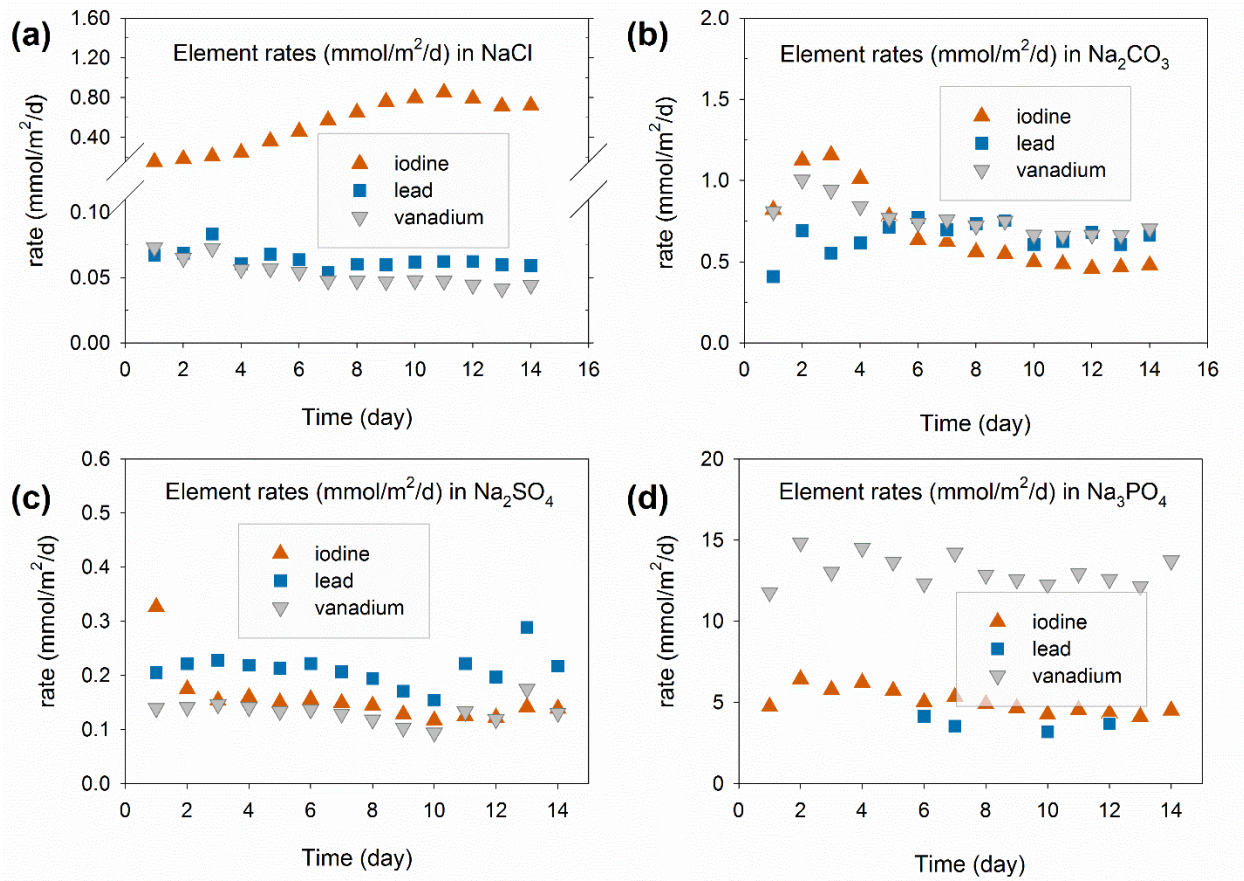


629

630 Figure 5. XRD phase analysis of the iodoapatite sample surface leached by 0.1
 631 mol/L NaCl solution. Two phases were identified: iodoapatite and vanadinite.

632

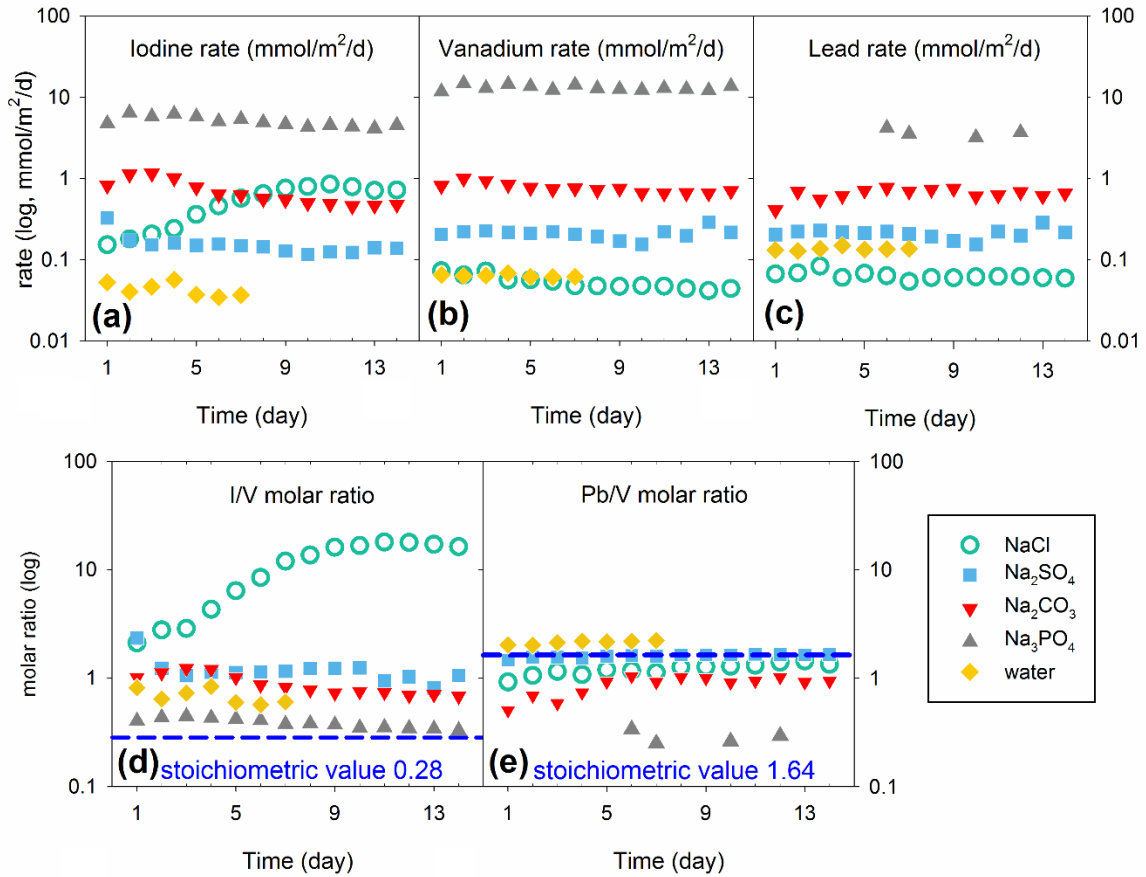
633



634

635 Figure 6. Solution analysis of collected leachates from 14 days semi-dynamic leach
636 tests on iodoapatite samples in (a) 0.1 mol/L NaCl, (b) 0.1 mol/L Na₂CO₃, (c) 0.1 mol/L
637 Na₂SO₄, and (d) 0.1 mol/L Na₃PO₄.

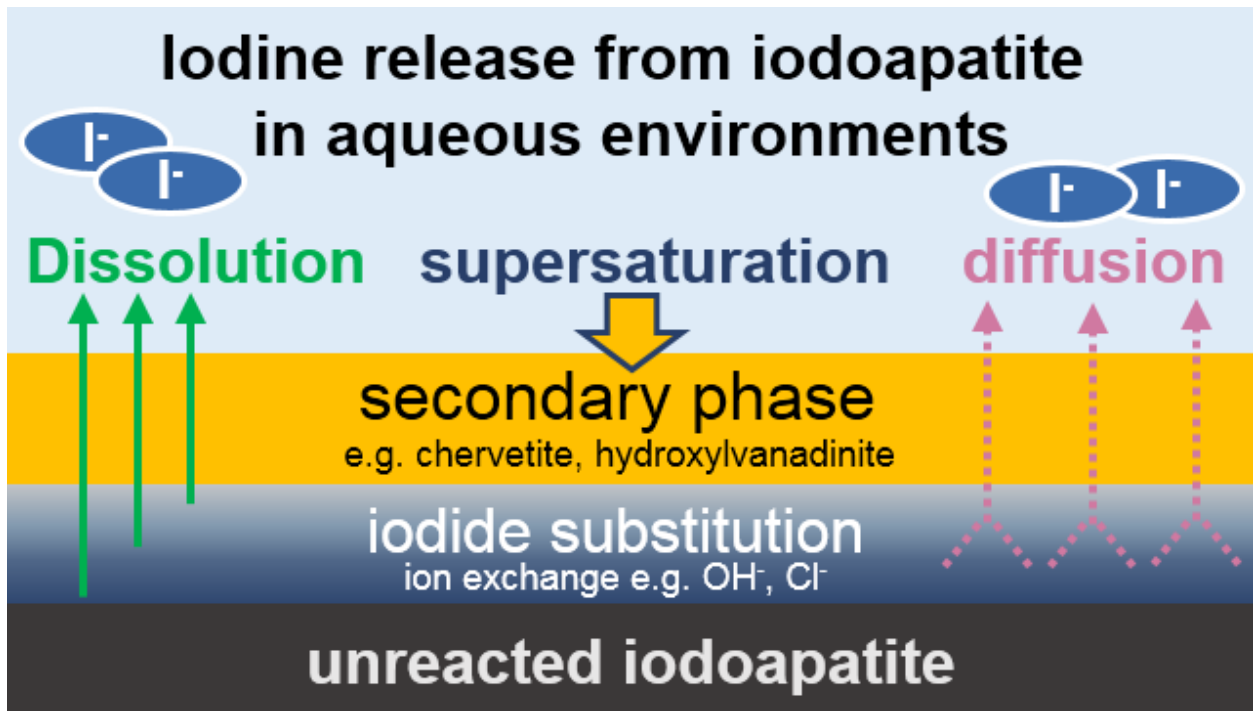
638



639

640 Figure 7. Comparison of element release rate of iodine (a), vanadium (b), and lead (c) in
 641 the leachate solutions from different leach tests. Molar ratios of Pb/V (d) and I/V (e) in
 642 leachate solutions from leach tests in NaCl, Na₂SO₄, Na₂CO₃, Na₃PO₄, and deionized
 643 water.

644



645

646

647

Figure 8. Schematic diagram illustrates major processes that control the iodine release from iodoapatite in aqueous environments

648 Table. 1 Crystallographic parameters based on the XRD refinements by Le Bail
 649 algorithm.

Leach test condition	Refined parameters				
	a, b (a=b, Å)	c (Å)	GoF	R _p (%)	R _{wp} (%)
Pristine	10.4420 (3)	7.4756 (3)	1.32	5.16	6.53
Water	10.4325 (3)	7.4864 (3)	1.63	6.04	7.73
0.1 mol/L Na ₂ SO ₄	10.4336 (2)	7.4837 (2)	1.39	4.60	5.93
0.1 mol/L Na ₂ CO ₃	10.1923 (2)	7.4656 (2)	1.65	4.85	6.44
0.1 mol/L Na ₃ PO ₄	10.1984 (2)	7.4449 (2)	1.43	4.74	6.23
0.1 mol/L NaCl (2 phases)	10.4443 (6)	7.4796 (5)	1.17	4.12	5.28
	10.3536 (8)	7.3735(8)			
Pb_{4.925}(VO₄)₃l_{0.85} [ICDD#04-011-4267]	10.422	7.467	Crystal system: hexagonal		
Pb₅(VO₄)₃(OH) [ICDD#01-075-7576]	10.2242	7.4537	Space group: P63/m #176;		
Pb₅(VO₄)₃Cl [ICDD#01-073-1732]	10.31	7.34	α=90° β=90° γ=120°		

650

651

652 Table 2. Solution chemistry at equilibrium state calculated by Visual MINTEQ under
 653 90 °C.

mol/L 90 °C	Deionized water	0.1 mol/L NaCl	0.1 mol/L Na ₂ SO ₄	0.1 mol/L Na ₂ CO ₃	0.1 mol/L Na ₃ PO ₄
pH (unitless)	6.1	6.1	6.2	10.3	10.9
Ionic strength	2.04×10^{-6}	0.098	0.26	0.25	0.29
Major cation	H⁺	Na⁺	Na⁺	Na⁺	Na⁺
Concentration	6.52×10^{-7}	0.098	0.18	0.18	0.22
Activity	6.51×10^{-7}	0.074	0.13	0.13	0.15
Activity coefficient	1.00	0.76	0.72	0.72	0.68
Major anion	OH⁻	Cl⁻	SO₄²⁻	CO₃²⁻	PO₄³⁻
Concentration	8.72×10^{-7}	0.098	0.079	0.069	0.012
Activity	8.70×10^{-7}	0.074	0.02	0.017	0.00049
Activity coefficient	1.00	0.76	0.25	0.24	0.041